ELSEVIER

Journal of Nuclear Materials 270 (1999) 87–95

journal of nuclear materials

Ramp test behavior of high O/U fuel

J.H. Davies *, E.V. Hoshi, D.L. Zimmerman

Vallecitos Nuclear Center, GE Nuclear Energy, 6705 Vallecitos Road, Sunol, CA 94586, USA

Received 29 April 1998; accepted 27 July 1998

Abstract

The effect of increased fuel oxygen potential on fuel behavior has been studied by fabricating and irradiating urania fuel with an average O/U ratio of 2.05. The fuel was fabricated by re-sintering standard urania pellets in a controlled oxygen potential environment and irradiated in a segmented rod bundle in a US BWR. Pre-irradiation ceramographic characterization of the pellets revealed the well-known Widmanstätten precipitation of U_4O_9 platelets in the UO_2 matrix. The high O/U fuel pellets were clad in Zircaloy-2 and irradiated to over 20 MWd/kgU. Ramp tests were performed in a test reactor and detailed post-irradiation examinations of both ramped and non-ramped rods have been performed. The cladding inner surface condition, fission gas release and swelling behavior of high O/U fuel have been characterized and compared with standard UO_2 pellets. Although fuel microstructural features in ramp-tested high O/U fuel showed evidence of higher fuel temperatures and/or enhanced transport processes, fission gas release to the fuel rod free space was less than for similarly tested standard UO_2 fuel. However, fuel swelling and cladding strains were significantly greater. In spite of high cladding strains, PCI crack propagation was inhibited in the high O/U fuel rods. Evidence is presented that the crystallographically oriented etch features often noted in peripheral regions of high burnup fuels are not an indication of higher oxides of uranium.

PACS: 28.41.B; 62.40.M

1. Introduction

An important consideration for high burnup fuel designs is the evolution of the fuel chemistry and, in particular, the fuel oxygen potential. Early GE measurements and other experimental results [1,2] indicate that LWR fuel oxygen potentials up to approximately 40 MWd/kgU are controlled by cladding oxidation, but at higher burnups, if cladding oxidation becomes kinetically limited, and with an increasing fraction of Pu fissions, an increase in fuel oxygen potential might be expected. Increasing oxygen potential can affect several important fuel properties, including thermal conductivity, fission gas release and creep behavior.

The effect of increased fuel oxygen potential has been studied here by fabricating and irradiating urania fuel with an average O/U ratio of 2.05.

2. Fabrication

The hyperstoichiometric UO_2 fuel pellets were produced by equilibrating batches of standard pellets in a CO_2/CO gas mixture (7:1 ratio) at 1400°C for 6 h in a small laboratory furnace followed by a rapid quench to below 800°C. Post-anneal measurements indicated a range of O/U ratios between 2.03 and 2.06, due largely to a temperature gradient over the length of the pellet stack in the furnace hot zone and to finite quench times. Consistent with the literature [3], the as-fabricated microstructure of the hyperstoichiometric UO_2 fuel showed two phases – a U_4O_9 phase in a UO_2 matrix.

Mean pellet density was 96.7% of theoretical and the true grain size averaged 24 μm.

* Corresponding author. Tel.: +1-925 862 4347; fax: +1-925 862 4515; e-mail: john.davies@gene.ge.com.

0022-3115/99/$ – see front matter
PII: S0022-3115(98)00756-9

Table 1
Test fuel segment description

Fuel pellets	
Fuel material	Hyperstoichiometric Urania
Composition	$UO_{2.03-2.06}$
Enrichment (w/o U^{235})	2.87
Density (g/cm^3)	10.59
Pellet geometry	Chamfered with flat end faces
Diameter (mm)	10.87
Length (mm)	10.7
Cladding	
Material	Zircaloy-2
Heat treatment	Recrystallization anneal
Outside diameter (mm)	12.52
Wall thickness (mm)	0.71
Inner surface finish	Etched
Segment	
Fill gas	Helium
Pressure (atm)	17
Pellet-clad gap (mm)	0.23
Hydrogen getter in plenum	Yes

The pellets were loaded into fuel rod segments and irradiated in a segmented test rod (STR) assembly in a US BWR. The design and irradiation of the GE segmented rods and STR assemblies have been described in the previous literature [4,5]. The specific design features of the test segments in the current study are shown in Table 1. The segments were irradiated at low power for up to five reactor cycles. They were retrieved and returned to the GE Vallecitos hotcells for characterization. Segment burnups were determined by Cs^{137} gamma scanning. Base irradiation and burnup data are summarized in Table 2.

3. Ramp testing

Two of the rods, STR111 and STR110, were power ramp tested in the Studsvik R2 reactor. Selected ramp test sequences are depicted in Fig. 1. The STR111 rod was subjected to a B sequence ramp and STR110 to an A ramp followed by a C ramp. Ramp terminal levels (RTLs) and hold times are given in Table 3; axial power profiles at RTL are superimposed on the rod burnup profiles in Figs. 2 and 3. Standard, non-barrier UO_2 fuel rods subjected to such severe power ramps have been shown to fail with a high probability [5], but the two rods tested here survived a total of three ramps without a failure indication. The soundness of the rods was confirmed by post-irradiation examination.

The third rod, STR113, was not ramp-tested.

4. Post-irradiation examination

4.1. Non-destructive

Post-irradiation examinations included neutron radiography, gamma scanning, diameter profilometry and eddy current flaw detection.

Neutron radiographs were taken of each rod at a single orientation to determine if there was hydrogen in the getters (a reliable indicator of rod failure) and to provide qualitative information on the states of the fuel pellet stacks. There was no evidence of getter hydriding, confirming that the rods were sound; but there was obvious centerline voiding in the B and A ramp regions of the ramp-tested rods, STR111 and STR110, respectively. The fuel stack in STR113 appeared undisturbed.

Gross gamma scans (>0.5 MeV) of the ramp-tested rods showed unusual peaks in the high power regions of STR110, most obviously in the region of the centerline voiding. At the time the gamma scans were performed, Cs^{137} plus Cs^{134} comprised a very large fraction of the total gamma activity and it was judged that the gross gamma scans essentially reflected the axial distributions of cesium. The gross gamma scan of STR113 was a relatively smooth curve, reflecting the axial burnup distribution along the rod.

The lower burnup rod (STR111) was scanned with a pulsed eddy current device and showed no indication of significant cladding flaws. The higher burnup rods (STR110 and STR113) were tested using continuous wave eddy current equipment with a calibrated encircling coil capable of detecting cladding defects. The eddy current trace on STR113 was clean and free of activity, indicating an absence of significant cladding defects. However, numerous large signals were detected on STR110 spanning the A ramp peak power region, and

Table 2
Power reactor irradiation

Serial number	STR111	STR110	STR113
Segment axial location	Lower middle	Bottom	Top
Number of irradiation cycles	2	5	5
Maximum peak power (W/cm)	174	193	131
Average/peak burnup (MWd/kgU)	9.0/9.7	20.9/24.9	17.1/21.8

lower levels of signal activity were noted towards the bottom of the rod in the C ramp region.

Helical and linear diameter profiles were recorded and, in the cases of STR111 and STR110, compared with profilometry data collected prior to ramp testing. Both rods exhibited significant diameter increases, including large ridging strains, in the ramp-tested regions. Maximum mid-pellet strains were estimated to be 0.24% for STR111 and 0.93% and 0.24% in the A and C ramp regions of STR110.

4.2. Destructive

The ramp-tested rods were punctured and the fission gases were collected and analyzed. The measured fission gas release fractions in STR111 and STR110 were 0.082 and 0.104, respectively.

The rods were sectioned to provide samples for ceramographic and metallographic characterization of the fuel and cladding with emphasis on characterizing the microstructures of the ramp-tested rods and under-

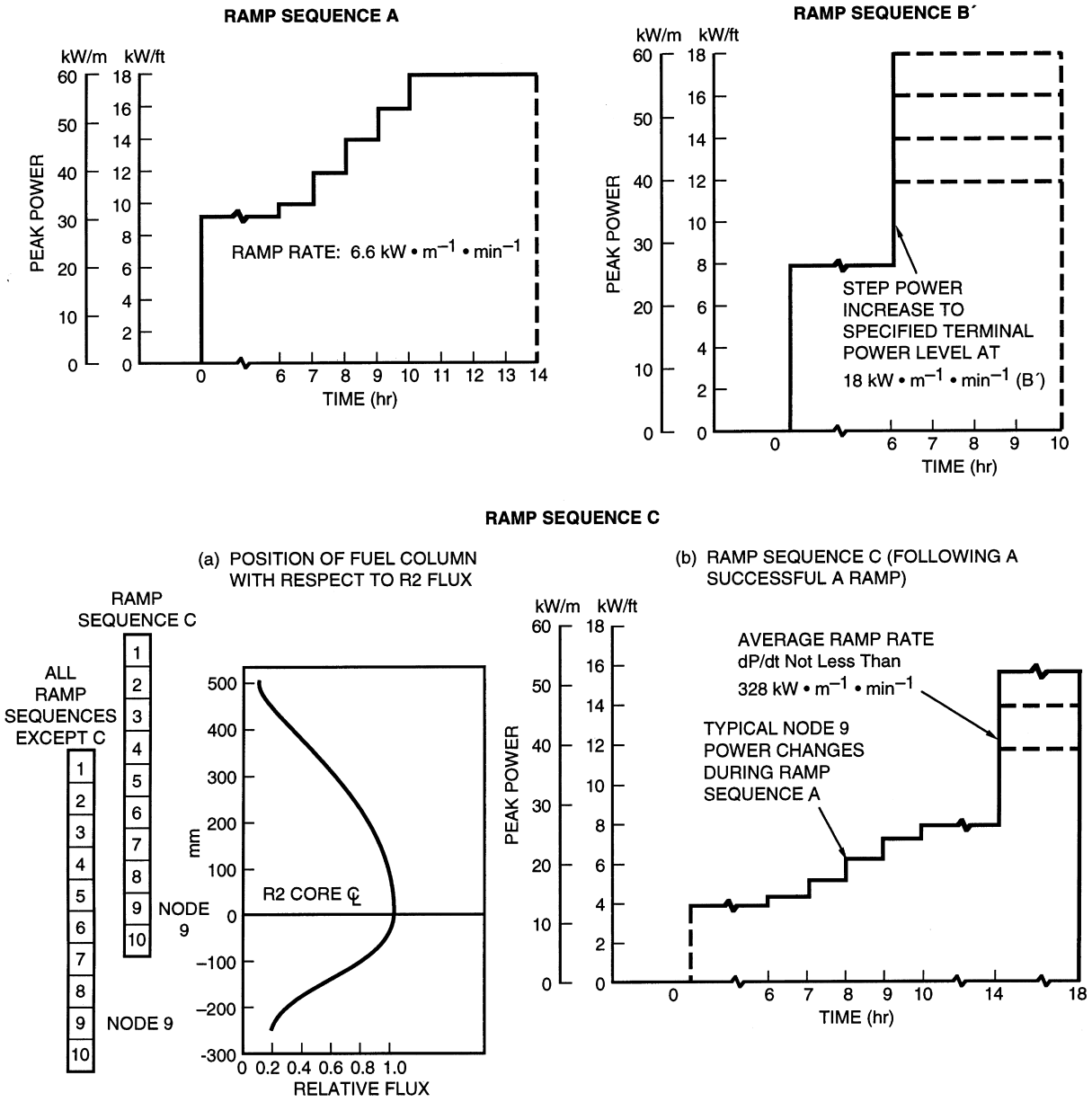

Fig. 1. Power ramp sequences.

Table 3
Ramp tests (rods sound)

First ramp					Second ramp			
Rod number	Ramp sequence [a]	Local BU (MWd/kgU)	RTL [b] (W/cm)	HT [c] (min)	Ramp sequence [a]	Local BU (MWd/kgU)	RTL [b] (W/cm)	HT [c] (min)
STR110	A	21.9	590	240	C	12.6	528	240
STR111	B	9.5	590	360	–			

[a] Ramp sequences shown in Fig. 1.
[b] Ramp terminal power level (RTL).
[c] Hold time (HT).

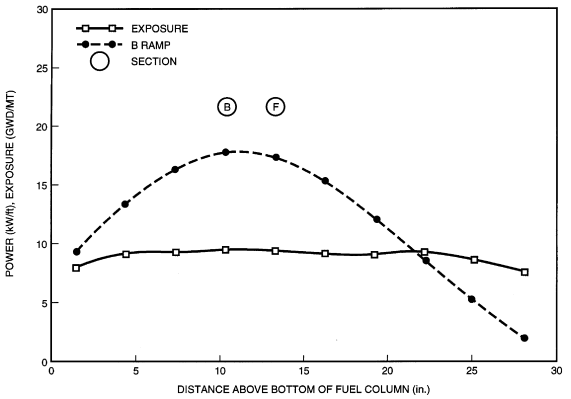

Fig. 2. STR111 nodal power/burnup profile.

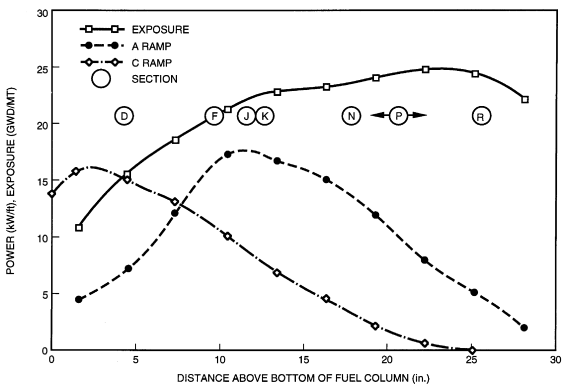

Fig. 3. STR110 nodal power/burnup profile.

standing the eddy current signal activity induced in STR110. The axial locations of selected sections are shown in Figs. 2 and 3. Two samples from the non-ramped rod (STR113) were also examined.

The cladding clamshell Section (P) of STR110 was interesting inasmuch as the pellets, which had operated up to 410 W/cm, were virtually intact and easily removed from the clamshelled tube; the pellets were not adhered to the cladding. Although the usual imaging of cracks and pellet interfaces was visible, contrast was poor due to the formation of a uniform oxide film on the cladding inner surface (Table 4).

Transverse sections at the ramp peak power locations of both ramped rods confirmed the formation of centerline voids. A photomacrograph of STR111 Section B is shown in Fig. 4. Extensive fuel restructuring is evident with a central void surrounded by columnar grains out to approximately mid-radius. The center void in STR110, examined in longitudinal section (Section J), was rough and uneven, indicating that it was still evolving and the RTL hold time (4 h) was too short to achieve steady-state conditions. There was no center void at the C ramp peak location of STR110 (Section D), confirming interpretation of the neutron radiograph, but columnar grain growth extended out to mid-radius. Beyond the columnar grain region in the restructured samples was an annulus of fission gas bubbles, which extended somewhat on etching, surrounded by an annulus of radially cracked, but largely unrestructured fuel. Porosity estimates indicated substantial fission gas bubble swelling in the restructured fuel.

Table 4
Cladding inner surface oxide thickness measurements

Rod number	Section	Description	Inner surface oxide thickness (μm)		
			Max	Min	Mean
STR111	B	Continuous	3.9	1.8	2.7
	F	Continuous			2.1
STR110	D	Continuous	9.3	4.3	6.5
	K	Continuous	7.8	4.1	5.7
	N	Continuous	10.7	6.3	7.0
	R	Continuous	8.5	4.6	6.4
STR113	C	Patch oxide	4.8	0	<1

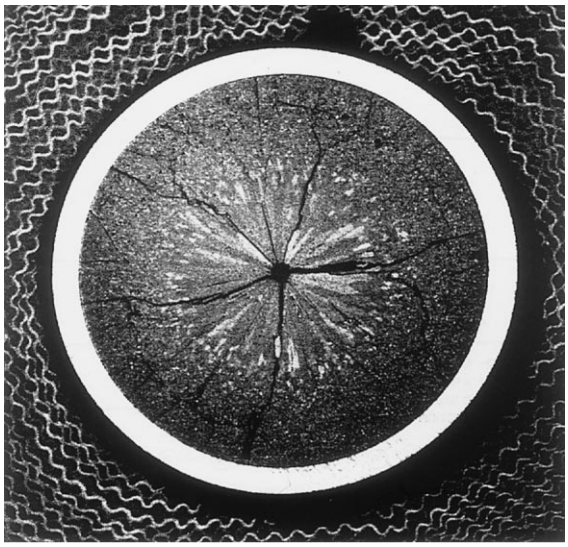

Fig. 4. STR111 Section B – showing center void and fuel restructuring.

STR110 Section K was taken close to the A ramp peak power location. The permanent (mid-pellet) cladding strain was 0.93% and the eddy current trace recorded large signals at this location. Metallographic examination of the cladding showed that the eddy current sensor was integrating and recording the effects of numerous incipient pellet cladding interaction (PCI) cracks that were observed all around the inner surface of the cladding. Approximately 130 cracks with greater than 10 μm penetration were noted. The maximum measured penetration was 97 μm; the mean penetration of cracks over 10 μm was 20.4 μm. The cracks appeared to be randomly distributed around the entire circumference. A typical area is illustrated in Fig. 5.

Similar incipient cracks were noted in STR110 Section D, taken close to the C ramp peak power (545 W/cm) location, where eddy current signals indicated possible cladding flaws, and in Section N (452 W/cm), where there were no eddy current indications. In Section D there were 53 cracks greater than 10 μm deep around the cladding inner surface, the deepest being 58 μm. Crack morphology varied from tight branching cracks to an open crack showing signs of local cladding strain. In Section N a total of 22 cracks were documented, mainly in two clusters at 0° and 160°; maximum crack penetration was ~100 μm. A picture emerges of hundreds of non-penetrating PCI cracks in the cladding wall over the approximately 17-inch axial span of the permanent cladding strain region.

The cladding inner surfaces of all the ramped rod sections examined, including STR110 Section R, which was remote from the ramp test region, had developed relatively thick oxide films, but there was no fuel-clad bonding. In contrast, for the non-ramped rod (STR113) there were oxide patches but no measurable inner surface oxide over two-thirds of the circumference. Oxide thickness measurements are summarized in Table 4.

Fuel microstructures were examined in the as-polished and etched conditions. Notably absent from all sections, both ramped and non-ramped, were the Widmanstätten structures, indicative of mixed UO_{2+x} plus U_4O_9 phases, which were documented in the as-fabricated fuel. However, there did appear to be differences from standard UO_2. Ceramographic preparation was difficult. Grain boundary cracking was evident in peripheral fuel in the as-polished condition and grain dropout during etching was severe. This was partly due to big differences in the etch times needed to develop

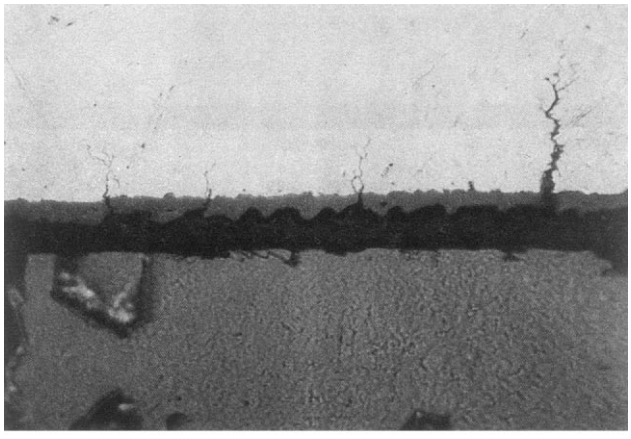

Fig. 5. STR110 Section K – incipient PCI cracks and cladding inner surface oxide layer (~370 ×).

grain boundaries at different radial locations, peripheral fuel being the most sensitive to etching and central regions the least.

In the course of investigating the fuel microstructures, an archive pellet was examined in a scanning electron microscope in both a chemically etched and cathodically etched condition. The Widmanstätten structure of U_4O_9 precipitates in the UO_2 matrix was revealed in both conditions. Careful examination of the chemically etched surface (Fig. 6) showed that the precipitates had etched proud of the matrix (i.e., the Widmanstätten pattern of precipitation projected out of the UO_2 surface). This observation has proved useful in interpreting the microstructural features in high burnup fuels. Acicular or platelet-like precipitates observed in peripheral regions of high burnup fuels after chemical etching have been suggested to be U_4O_9 precipitates within the UO_2 matrix and taken as direct evidence of fission-induced excess oxygen in the fuel. But these acicular features are not developed by cathodic vacuum etching, whereas it has been shown here that U_4O_9 precipitates in UO_2 are developed by cathodic etching, albeit with less definition than the chemical etch. Moreover, the U_4O_9 precipitates etch proud of the UO_2 matrix, whereas the irradiated fuel acicular features are etch pits in the surface.

4.3. Fractography

The fracture surfaces of some incipient PCI cracks were prepared for examination as follows. A ring of STR110 cladding was defueled and cut into arc samples. A selected cladding arc was then fractured longitudinally by subjecting it to a compressive radial loading in a shop vise. Examination of the fracture surfaces at low magnification showed two distinct regions: (a) a darker band penetrating to a depth of between 50 and 115 μm from the cladding inner surface and (b) a lighter region. The inner band extended the entire length of the sample, which was 6.4 mm. Examined at higher magnification, the fracture mode of this inner band was mostly intergranular (Fig. 7), indicative of stress corrosion cracking; the remaining fracture surface had a dimpled appearance, which is characteristic of ductile rupture caused by mechanically fracturing the sample.

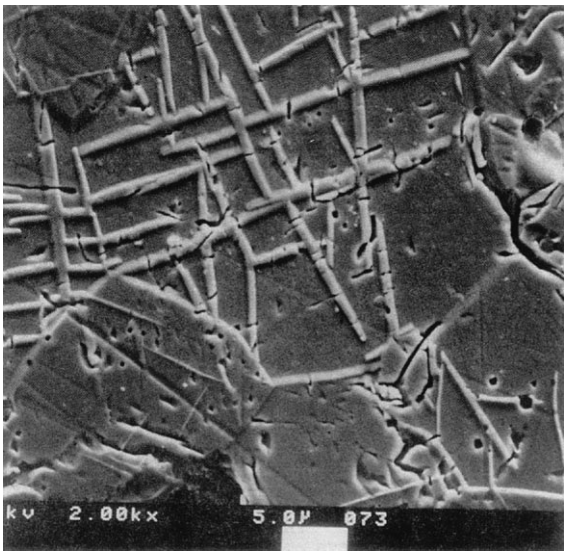

Fig. 6. SEM micrograph of unirradiated archive fuel pellet.

5. Discussion

The diameter profilometry, neutron radiogaphy and fission gas release measurements from the ramp-tested rods have been compared and contrasted with similarly tested standard UO_2 rods employing GE zirconium barrier cladding.

Maximum mid-pellet strains are compared in Table 5. The strain recorded in the A ramp region of STR110 is much higher than previous experience. The C ramp region was at a lower burnup and experienced a lower RTL (Fig. 3); STR111 was a lower burnup rod.

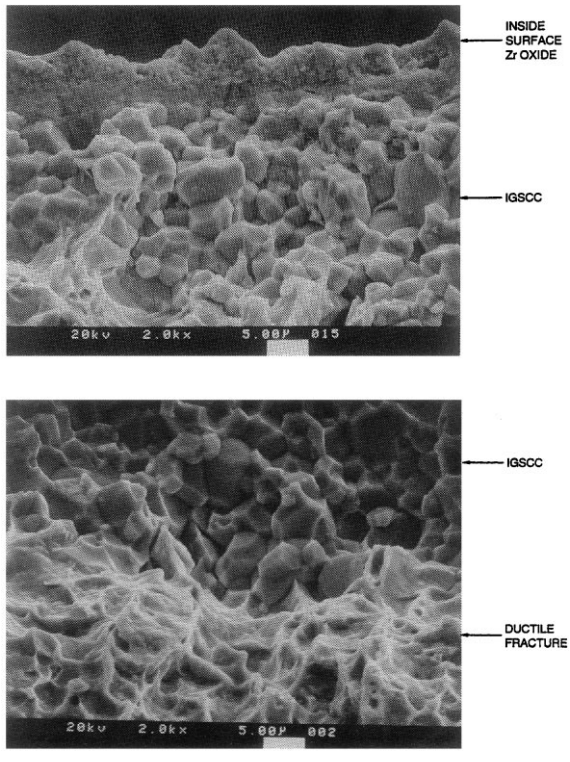

Fig. 7. SEM micrographs of fracture surface of cladding section.

Table 5
Permanent cladding strains from standard and hyperstoichiometric UO_2 fuel rods tested under similar conditions

Rod No.	Fuel	Local. burnup (MWd/kgU)	Type ramp	RTL (W/cm)	Hold time (min)	Maximum mid-pellet strain (%)
SRP-3/70	Standard UO_2	26.2	C	590	240	0.53
SRP-3/71	Standard UO_2	28.8	A	590	240	0.63
		27.6	C	585	240	0.41
STR110	Hyperstoich. UO_2	21.9	A	590	240	0.93
		12.6	C	528	240	0.24
SRP-3/20	Standard UO_2	6.7	B	595	360	0.16
SRP-3/44	Standard UO_2	6.4	B	595	360	0.04
SRP-3/45	Standard UO_2	6.2	B	595	360	0.1
SRP-3/46	Standard UO_2	7.8	B	595	360	0.08
SRP-3/47	Standard UO_2	7.7	B	595	360	0.14
STR111	Hyperstoich. UO_2	9.5	B	595	360	0.24

Ohara et al. [6] have reported the cladding strains on similarly ramp-tested rods as a function of RTL and burnup. Referring to Ohara's results, the A ramp strain on STR110 is roughly equivalent to that of a standard UO_2 rod at twice the burnup.

The existence of center voiding, as evidenced from neutron radiography (confirmed by destructive examinations), also contrasts with experience with standard UO_2. Of many standard fuel rods ramp-tested to 590 W/cm and neutron radiographed, only one instance of 'possible center voiding' was noted [5]. Fuel sections that had operated at 590 W/cm exhibited substantial grain growth and distinctive zones of porosity distribution, but center voiding was not observed. The effect of the excess oxygen in hyperstoichiometric UO_2 in promoting center void formation is believed to be twofold: (1) it reduces the fuel thermal conductivity, giving rise to higher center temperatures; and (2) it enhances the vaporization-condensation processes in the temperature gradient, which lead to void formation. Both of these effects have been discussed by Olander [7].

Measured fission gas release fractions are compared with those of similarly ramp-tested standard UO_2 rods in Table 6. In spite of the significant fuel restructuring in STR110, the fission gas release was relatively low compared to the standard fuel. However, this result is consistent with the high fuel swelling in STR110 manifested by the high cladding strain and estimates of fuel porosities.

The high cladding strains on the ramp-tested rods imply severe duties, yet the rods were sound. However, large eddy current signals on STR110 were an indication of cladding flaws or defects. This was confirmed by destructive examination which showed that the defect signals were caused by very many incipient or non-penetrating PCI cracks. Some of the cracks exhibited significant opening displacement, but maximum crack penetrations of 100–115 μm were not exceeded. Preparation and examination of fracture surfaces showed the fracture mode to be largely intergranular, confirming the stress corrosion cracking (SCC) mechanism determined to be the cause of PCI cracks in Zircaloy cladding ma-

Table 6
Fission gas release from standard and hyperstoichiometric UO_2 fuel rods tested under similar conditions

Rod No.	Fuel	Local. burnup (MWd/kgU)	Type ramp	RTL (W/cm)	Hold time (min)	FGR fraction
SRP-2/38	Standard UO_2	14.5	A	587	240	0.193
			C	574	240	
SRP-2/43	Standard UO_2	10.7	A	587	240	0.164
			C	626	240	
SRP-2/45	Standard UO_2	11.2	A	594	240	0.189
			C	600	240	
SRP-3/95	Standard UO_2	16.3	A	594	240	0.132
			C	525	240	
SRP-3/97	Standard UO_2	17.8	A	600	240	0.17
			C	522	240	
STR110	Hyperstoich. UO_2	20.9	A	590	240	0.104
			C	528	240	
STR111	Hyperstoich. UO_2	9.0	B	590	360	0.082

terials. Fracture mode can be revealing about the development of PCI cracks. Cox [8] and others have noted small amounts of intergranular cracking near the origins of SCC cracks turning to transgranular fracture as propagation ensued. Videm and Lunde [9] studied SCC crack growth rates as a function of stress intensity and showed (Fig. 8) that purely intergranular SCC was favored by slow rates of propagation and transgranular SCC by rapid propagation. Mixed mode fracture is an intermediate case.

From the large number of incipient PCI cracks in STR110, it appears that hyperstoichiometric UO_2 is effective in inhibiting crack propagation, but not crack initiation. Furthermore, given the severe cladding strains and the observation of some crack opening, crack propagation is not inhibited by any amelioration of the pellet-cladding mechanical interaction. It appears, therefore, to be a chemical effect. It is hypothesized that oxygen is effectively blocking the transport of the embrittling species, presumably iodine, to the crack tip.

The influence of oxygen in iodine SCC of Zircaloy has been studied out-of-pile. Wood [10] concluded that oxygen was a catalyst for SCC. Conversely, Une, as referenced by Cox [11], has reported that oxygen inhibits SCC by competing for active sites. Gangloff et al. [12] studied the influence of oxygen on iodine embrittlement of Zircaloy and zirconium. Oxygen influenced crack initiation by eliminating the general pitting attack observed in pure iodine. Crack initiation and early growth was predominantly intergranular.

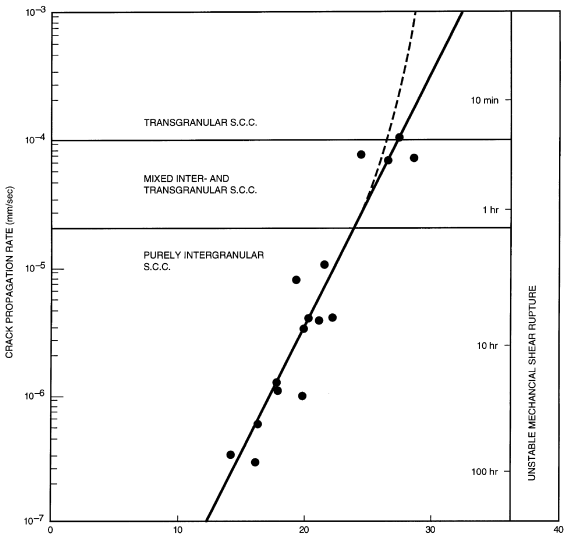

Fig. 8. Stress corrosion crack growth rate as a function of stress intensity for fatigue precracked cladding tubes. Test temperature 340°C. 3 mg/cm^3 of iodine was added initially. Fully recrystallized cladding tubes [9].

It is difficult to know either the concentration of the embrittling species or the oxygen in the ramped hyperstoichiometric UO_2 fuel rods. But, by comparison to the unramped rod (STR113), it is apparent that almost all of the 6 μm inner surface oxide layer was formed during the ramp test (4-h hold at RTL). The largely intergranular fractures are consistent with those observed by Gangloff et al. [12] in a mixed iodine plus oxygen environment and, according to Videm and Lunde's criteria (Fig. 8), crack propagation was relatively slow. The absence of penetrating cracks may simply be a consequence of the propagation rate in an oxidizing environment, being too slow to be sustained by a limited or transitory burst release of embrittling fission product species. That is, the time for crack penetration is longer than the 'decay constant' of the active species.

The absence of the as-fabricated Widmanstätten precipitation pattern from the irradiated fuel structures is puzzling and appears to be more than simply the quenching in of single phase UO_{2+x} due to rapid cooling of the fuel. Perhaps the concentration of foreign atoms in the UO_{2+x} matrix inhibits the phase transformation to UO_2 plus U_4O_9.

The SEM characterization of unirradiated hyperstoichiometric UO_2 fuel showed that the U_4O_9 precipitates etched more slowly than the UO_2 matrix. Thus, the Widmanstätten pattern of precipitation projects out of the UO_2 matrix, arguing against the hypothesis that the crystallographically oriented etch features noted in high burnup fuel are U_4O_9 precipitates. It seems more likely that the acicular features are defects or intragranular microcracks on {1 1 1} crystal habit planes, as described by Thomas et al. [13].

Acknowledgements

The high O/U fuel pellets were fabricated by D.E. Owen. The ramp test of the STR111 rod was performed under a program sponsored by the US Department of Energy. Much of the post-irradiation examination work was funded by Tokyo Electric Power Company.

References

[1] M.G. Adamson et al., Oxygen redistribution and its measurement in irradiated oxide fuels, in: Proceedings of the IAEA Symposium on Thermodynamics of Nuclear Materials, Vienna, 21–25 October, 1974, p. I-59.
[2] H. Kleykamp, J. Nucl. Mater. 84 (1974) 109.
[3] B.E. Schaner, J. Nucl. Mater. 2 (1964) 110.
[4] J.H. Davies, Power ramp tests of potential PCI remedies, in: Proceedings of the ANS Topical Meeting on LWR Fuel Performance, Portland, OR, 29 April–2 May, 1979, p. 275.

[5] J.H. Davies et al., Fuel Ramp Tests in Support of a Barrier Fuel Demonstration, General Electric Company, July 1984 (GEAP-22076).
[6] H. Ohara, Fuel behavior during power ramp tests, in: Proceedings of the ANS International Meeting on LWR Fuel Performance, West Palm Beach, FL, 17–21 April 1994, p. 674.
[7] D.R. Olander, Fundamental Aspects of Nuclear Reactor Fuel Elements, TID-26711-P1, reprinted by Technical Information Center, US Department of Energy, 1976.
[8] B. Cox, J. Nucl. Mater. 170 (1990) 1.
[9] K. Videm, L. Lunde, Stress Corrosion Crack Initiation and Growth in Zircaloy, paper presented at OECD Enlarged Halden Group Meeting, Sanderstolen, Norway, 1977.
[10] J.C. Wood, J. Nucl. Mater. 45 (1972) 105.
[11] B. Cox, J. Nucl. Mater. 172 (1990) 249.
[12] R.P. Gangloff, D.E. Graham, A.W. Funkenbusch, Corrosion 35 (1979) 316.
[13] L.E. Thomas, J. Nucl. Mater. 166 (1989) 243.